Electrochemistry
The Electrochemical Society of Japan
Received: November 19, 2021
Accepted: January 5, 2022
Published online: January 12, 2022
Issued: February 11, 2022
https://doi.org/10.5796/electrochemistry.21-00121
Note
Electrochemistry, 90(2), 027004 (2022)

Electrochemical Properties of Cs and La Co-doped $CaWO_4$ Oxide Ion Conductor

Shigeomi TAKAI,[a,*,§] Ryo TAKEMOTO,[b] Takeshi YABUTSUKA,[a] and Takeshi YAO[c,§]

[a] Graduate School of Energy Science, Kyoto University, Yoshida-Honmachi, Sakyo-ku, Kyoto 606-8501, Japan
[b] Graduate School of Engineering, Tottori University, Koyama-cho Minami, Tottori 680-8552, Japan
[c] Processor Emeritus, Kyoto University, Yoshida-Honmachi, Sakyo-ku, Kyoto 606-8501, Japan

* Corresponding author: stakai@energy.kyoto-u.ac.jp

ABSTRACT

To clarify the contribution of defect structure of $CaWO_4$-based system on the oxide ion conduction properties, we doped both cesium and lanthanum ions into $CaWO_4$ as $Ca_{0.9}Cs_xLa_{0.1-x}WO_{4.05-x}$. Scheelite-type structured solid solution can be obtained for the Cs-rich region ($x \geq 0.05$) with oxygen deficiency, while second phase appears for La-rich region ($x \leq 0.025$) assuming excess oxide ions. In the present system, a bend in Arrhenius plot of conductivity is observed around 850 °C as the typical $CaWO_4$-based system even co-doping with La ions. In terms of the compositional dependence, ionic conduction develops from $x = 0.05$ with the amount of cation vacancy below 800 °C, while the conductivity enhancement starts at the La-rich region above 900 °C. This indicates that not only oxide ion vacancy but also interstitial attribute to the oxide ion conduction at high-temperature, which is also suggested by the activation energy.

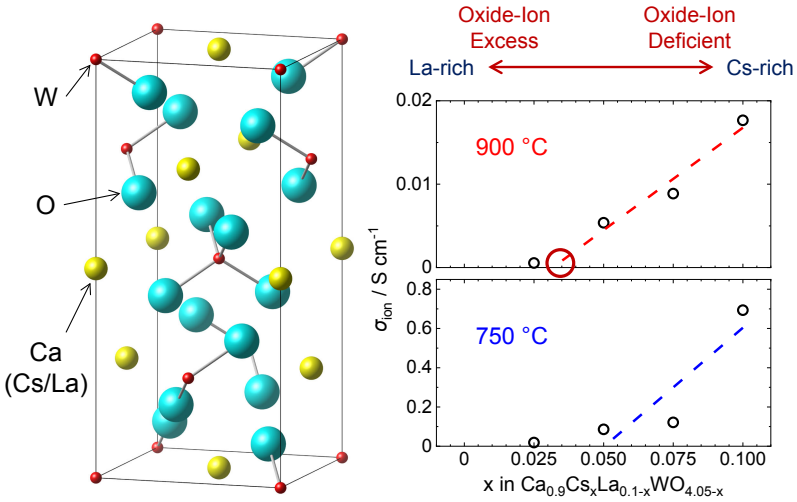

Keywords : Oxide Ion Conductor, Scheelite, $CaWO_4$, Defect Structure

1. Introduction

Oxide ion conductors have been attracted great interests for the application of electrolytes of solid oxide fuel cells (SOFCs).[1,2] Sceelite-type structured compounds with the form of ABO_4 are promising candidates for base materials of the series of oxide ion conductors. Some of these materials represent oxide ion conduction by introducing the excess oxide ions at interstitial site. For example, when trivalent La^{3+} ions are partly substituted for Pb^{2+} site of $PbWO_4$, oxide ion interstitials are created as $Pb_{1-x}La_xWO_{4+x/2}$ to exhibit a high oxide ion conduction at elevated temperature.[3–5] Similar enhancement in ionic conduction due to the oxide ion interstitials has been reported for other scheelite-type structured systems, such as $PbMoO_4$,[6] $CaMoO_4$,[7] $BaMoO_4$,[8] high-temperature form of $CeNbO_4$,[9] $LaNbO_4$,[10,11] or $GdNbO_4$.[12] However, $CaWO_4$ with mineral name of scheelite is unlikely to form solid solution by lanthanum substitution incorporating excess oxide ions at interstitial site.[1]

We have recently reported that monovalent ion can be substituted into $CaWO_4$ forming oxide ion vacancy as $Ca_{1-x}A_xWO_{4-x/2}$ (A = K or Cs), which also shows high oxide ion conduction at elevated temperature.[13,14] Oxygen gas and water vaper concentration cells revealed that the major charge carrier of this system is not proton but oxide ion. Although the scheelite-type structure is derived from the fluorite-type,[15] only few oxide ion conductors have been reported for oxygen deficient scheelite-type structure.[16] In addition to the defect structure, $CaWO_4$-based system shows a characteristic feature of temperature dependence of ionic conductivity, i.e. $CaWO_4$-based system exhibits the conductivity jump or drastic change in slope at Arrhenius plot around 600 °C–800 °C.[13,14] Nevertheless, considering that, in the oxygen-excess scheelite-type structured system, long-range oxide ion migration would pursue not only through the interstitial sites but also the regular sites,[11,17–19] oxide ion diffusion mechanism of vacancy-type as oxide-ion jump between the regular sites is thought to be related to that of interstitial-type. In the present study, we introduce both La^{3+} and Cs^+ ions into $CaWO_4$ as $Ca_{0.9}Cs_xLa_{0.1-x}WO_{4.05-x}$, in which the oxide-ion defect can be altered by the La/Cs rate keeping the total amount of dopant. The variation of ionic conduction properties of $CaWO_4$-based system is discussed in terms of the defect structure.

2. Experimental

$Ca_{0.9}Cs_xLa_{0.1-x}WO_{4.05-x}$ ($x = 0$, 0.025, 0.050, 0.075 and 0.10) samples were prepared by conventional solid state reaction method started from the stoichiometric mixture of $CaCO_3$, H_2WO_4, Cs_2CO_3

§ECSJ Active Member
S. Takai orcid.org/0000-0001-9067-0806
T. Yabutsuka orcid.org/0000-0003-2111-7470

and La_2O_3 reagents. The calcining and sintering temperatures were selected as 800 °C and 1000 °C, respectively. The crystalline phases of the prepared samples were identified by room-temperature powder X-ray diffraction (Rigaku, Ultima IV) with CuKα radiation (40 kV, 40 mA).

For the conductivity measurements, platinum paste was applied on both sides of the cylindrical sample (ϕ10 mm in diameter and 5–8 mm in length), and impedance measurements were carried out in the frequency range 5 Hz–5 MHz by means of two-electrode method using an impedance analyzer (Agilent 4192A).

Oxygen gas concentration cell was constructed using sample disc (ϕ10 mm in diameter and 1 mm in thickness) as an electrolyte to estimate the charge carrier of the sample. The cathode and anode gases supplied were pure oxygen gas ($P(O_2) = 1$ atm) and air ($P(O_2) = 0.21$ atm), respectively. The measured electric motive force (EMF) was compared with that estimated by Nernstian equation.

3. Results and Discussion

Figure 1 shows XRD patterns of the prepared $Ca_{0.9}Cs_xLa_{0.1-x}WO_{4.05-x}$, where La-rich ($x < 0.05$) and Cs-rich ($x > 0.05$) regions nominally correspond to the oxygen excess and deficient compositions, respectively. While single phase of scheelite-type structure is obtained in the Cs-rich region, small extra peaks of $La_{14}W_8O_{45}$ are detected in the La-rich region.[20] The impurity peaks grow larger with La-concentration or decreasing x as shown in the enlarged patterns in Fig. 1. This suggests that $CaWO_4$-based system is unlikely to involve the oxide ion interstitials,[3] although small amount of La ion can be substituted with an aid of co-doping with Cs ions as $x = 0.05$ or 0.075. Although the enlarged pattern for $x = 0.1$ seems to include small amount of impurity other than $La_{14}W_8O_{45}$, peak intensity of the impurity is much small and we considered the solid solution range of this system as $x \geq 0.05$. Arrhenius plot of electrical conductivity for $Ca_{0.9}Cs_xLa_{0.1-x}WO_{4.05-x}$ is represented in Fig. 2. All the samples exhibit higher conductivities in comparison with that of pure $CaWO_4$ and the conductivity increases with the cesium concentration x. Except for $x = 0$, a conductivity jump or change in slope is observed around 850 °C, which is the similar trend with $Ca_{1-x}Cs_xWO_{4-\delta}$ or $Ca_{1-x}K_xWO_{4-\delta}$ systems with oxygen deficiency.[13,14]

The EMF measurements of oxygen gas concentration cells were carried out using $Ca_{0.9}Cs_xLa_{0.1-x}WO_{4.05-x}$ as an electrolyte, and average transport numbers of ion are evaluated from the ratio of measured EMF of the cell E against E_o of the Nernstian values as $\bar{t} = E/E_o$, which are plotted in Fig. 3. Some data points just exceeded the unity of ionic transport number, which might be caused by the temperature-inhomogeneity in the sample due to the deviation of gas flow rate. Cs-rich samples of $x \geq 0.05$ possess the ionic transport number close to unity, whereas La-rich sample of $x = 0.025$ exhibits the lower transport number. Since the constant current can be drawn from the concentration cell, the major charge carrier is oxide ion for the samples with oxygen deficiency and the electronic contribution would appear in the oxygen excess composition. The ionic conductivity is deduced as $\sigma_{ion} = \bar{t} \cdot \sigma$ to plot in Fig. 4, where change in slope is still observed around 850 °C. Figure 5 shows the activation energies E_a obtained in the temperature range 600 °C–800 °C and 900 °C–1000 °C based on $\sigma T = A \exp(-E_a/(kT))$. The activation energy in the former (lower temperature) region gradually increases with x from 1 eV to 2 eV, while the latter remains around or below 0.5 eV.

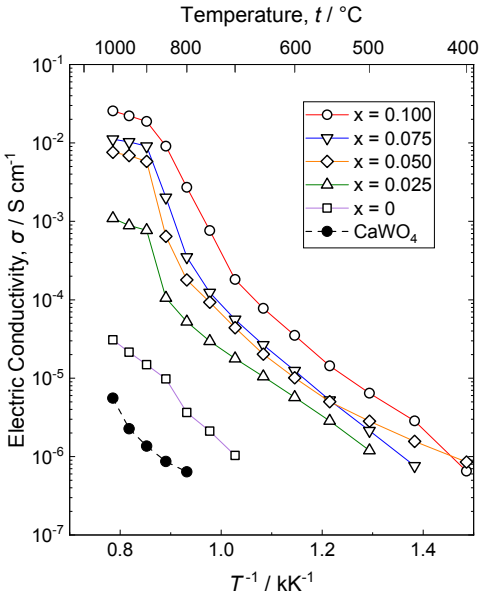

Figure 2. Arrhenius plots of electric conductivities for $CaWO_4$ (closed circle) and $Ca_{0.9}Cs_xLa_{0.1-x}WO_{4.05-x}$ (open symbols). □: $x = 0$, △: $x = 0.025$, ◇: $x = 0.050$, ▽: $x = 0.075$ and ○: $x = 0.1$.

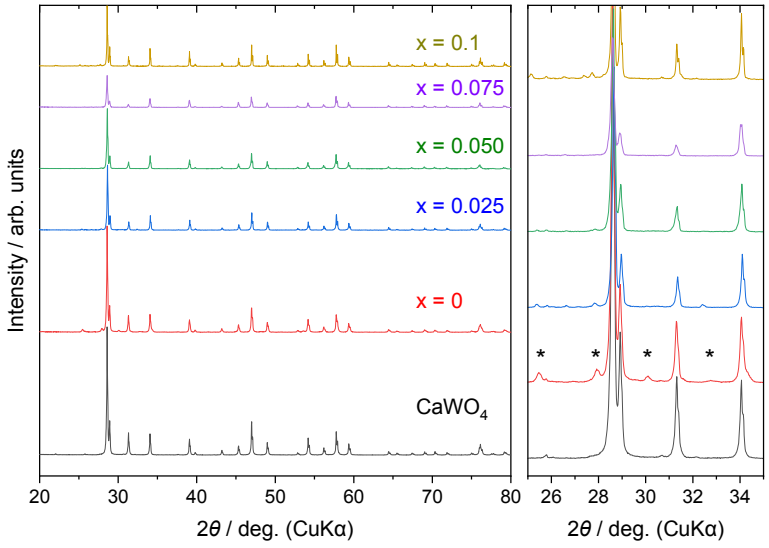

Figure 1. XRD patterns of $Ca_{0.9}Cs_xLa_{0.1-x}WO_{4.05-x}$ and $CaWO_4$ measured at room temperature. Enlarged profiles in the region $25° < 2\theta < 35°$ are also given at the right side, and diffraction peaks of $La_{14}W_8O_{45}$ are indicated by asterisks.

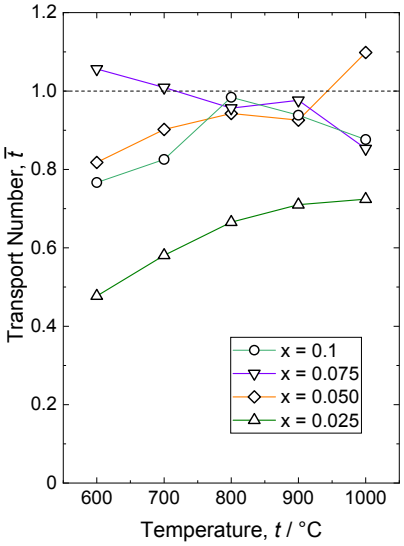

Figure 3. Ionic transport numbers evaluated from the EMFs of the following oxygen concentration cell, Air ($P(O_2) = 0.21$ atm) | $Ca_{0.9}Cs_xLa_{0.1-x}WO_{4.05-x}$ | Oxygen gas ($P(O_2) = 1$ atm) with the Nernstian value.

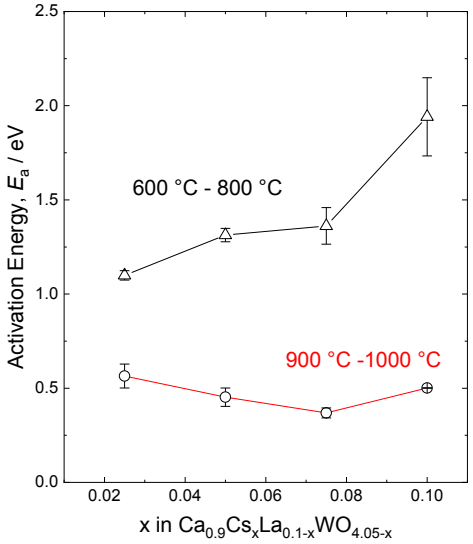

Figure 5. Activation energies of ionic conductivity calculated based on the data in the ranges 600 °C–800 °C (△) and 900 °C–1000 °C (○).

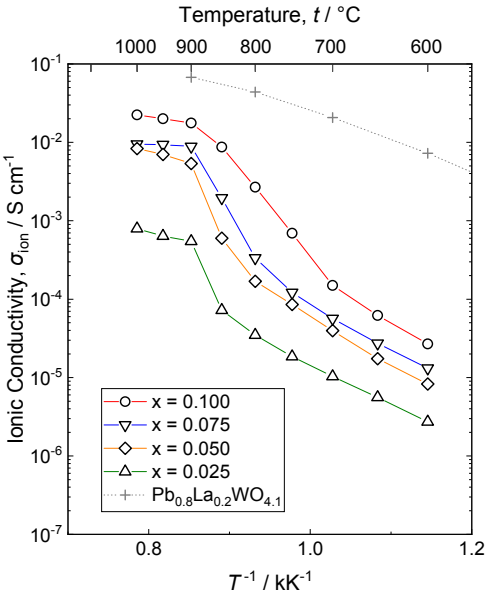

Figure 4. Arrhenius plots of ionic conductivity for $Ca_{0.9}Cs_x$-$La_{0.1-x}WO_{4.05-x}$ through the product of the electric conductivity in Fig. 2 and the average transport number estimated from the EMF ratio of oxygen gas concentration cell in Fig. 3. Conductivity data for $Pb_{0.8}La_{0.2}WO_{4.1}$ is also indicated by (+) symbol for the comparison.

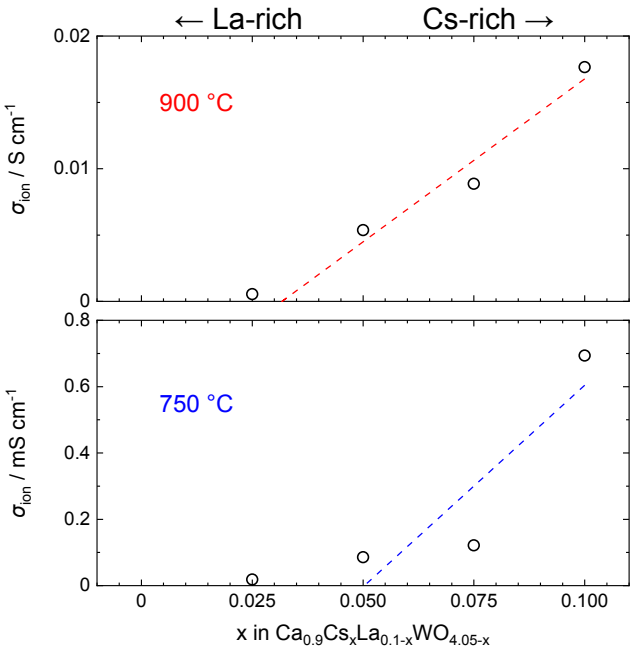

Figure 6. Ionic conductivity isotherms of $Ca_{0.9}Cs_xLa_{0.1-x}$-$WO_{4.05-x}$ obtained at 900 °C and 750 °C. The dashed lines are drawn by linier fitting using the data of Cs-rich region including $x = 0.05$.

To estimate the contribution of defect structure on the ionic conduction, compositional dependence of ionic conductivity has been compared. Figure 6 representatively shows the ionic conductivity isotherms at 750 °C and 900 °C. Assuming that the conductivity is proportional to the oxide ion vacancy concentration under the vacancy diffusion mechanism keeping the carrier mobility, the conductivity should linearly increase from $x = 0.05$ with x. The measured ionic conductivity appears to develop linearly with x in the Cs-rich region, while it remains small in the La-rich region. It is also observed that conductivity enhancement starts around $x = 0.05$ at 750 °C, although it rises in the La-rich region ($x \sim 0.03$) at 900 °C. Although the ionic conductivity of $x = 0.05$ in Fig. 5 appears to be higher than electrical conductivity of pristine $CaWO_4$ displayed in logarithmic scale in Fig. 2, it can be seen from Fig. 6 that oxide ion vacancy mainly attributes to oxide ion conductivity. Employing 3 data points in the Cs-rich composition ($x \geq 0.05$), a straight line is fitted to provide an intercept on x-axis, which is then plotted against temperature in Fig. 7. Note that data point at $x = 0.025$ is excluded for the fitting due to the possible contribution from the impurity. It is shown in Fig. 7 that the intercept remains approximately 0.05 below 850 °C, and it decreases down to 0.03 above 900 °C. When the oxide ions are partly displaced into the interstitial position leaving vacancy

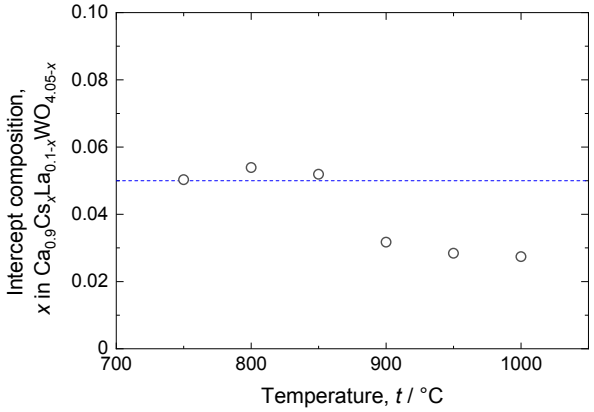

Figure 7. Intercept cesium concentration obtained from the compositional dependence of ionic conductivity in Fig. 6.

at the original site at high-temperature, the vacancy would be excessively introduced in comparison with the nominal value, and hence the ionic conductivity due to the vacancy diffusion would be enhanced to reduce the intercept x_o. If the oxide ion migrates through the interstitial position as above assumption at higher temperature, oxide ion diffusion path would be altered as the $PbWO_4$-based system with the oxide ion interstitials. This assumption is also supported by the change in activation energy in Fig. 5, since the activation energy 0.67 eV for $Pb_{1-x}La_xWO_{4+x/2}$ ($x = 0.2$) obtained above 700 °C is close to that of present system above 900 °C rather than below 800 °C.[3] Simply assuming that oxide ions are partly placed at the interstitial site and all regular oxide ion sites are just filled at the intercept composition x_o, the amount of oxide ion interstitials are roughly estimated as $0.05 - x_o$ for unit chemical formula. Even for the maximum in the present system, the interstitial oxide ion amount is approximately 0.02, which is much smaller than 0.10 for $Pb_{1-x}La_xWO_{4+x/2}$ ($x = 0.2$). Further investigation should be made using high-temperature neutron diffraction experiments coupled with maximum entropy method.

4. Conclusion

Cs and La co-doped $CaWO_4$ have been prepared as $Ca_{0.9}Cs_x$-$La_{0.1-x}WO_{4.05-x}$ to investigate the contribution of defect structure to the ionic conduction properties. Room temperature XRD experiments show the formation of solid solution for Cs-rich region with oxygen deficiency, while small amount of $La_{14}W_8O_{45}$ appears for La-rich samples with oxygen excess. Oxide ion conductivity increases with the Cs concentration, showing conductivity jump around 850 °C for most of the compositions. In the diagram of conductivity isotherm, σ_{ion} increases with the nominal oxide ion deficiency from $x = 0.05$ below 800 °C, while it starts to increase in the La-rich region above 900 °C. At high-temperature, the conduction properties of $CaWO_4$-based oxide ion conductors are supposed to be associated with the $PbWO_4$-based with oxide ion interstitials.

Acknowledgments

A part of this study has been performed with the late Prof. Takao Esaka (deceased in 2018) in Tottori University. This work was partly supported by JSPS KAKENHI Grant Number 17K06016.

CRediT Authorship Contribution Statement

Shigeomi Takai: Conceptualization (Lead), Data curation (Lead), Formal analysis (Lead), Funding acquisition (Lead), Investigation (Equal), Methodology (Equal), Project administration (Lead), Resources (Lead), Supervision (Lead), Validation (Lead), Visualization (Lead), Writing – review & editing (Lead)

Ryo Takemoto: Data curation (Equal), Formal analysis (Equal), Investigation (Lead), Methodology (Lead), Project administration (Supporting), Resources (Supporting), Visualization (Equal), Writing – review & editing (Supporting)

Takeshi Yabutsuka: Formal analysis (Supporting), Funding acquisition (Equal), Methodology (Supporting), Project administration (Supporting), Resources (Equal), Supervision (Equal), Writing – review & editing (Supporting)

Takeshi Yao: Formal analysis (Supporting), Funding acquisition (Equal), Methodology (Supporting), Project administration (Supporting), Resources (Supporting), Supervision (Equal), Validation (Supporting), Writing – review & editing (Supporting)

Conflict of Interest

The authors declare no conflict of interest in the manuscript.

Funding

Japan Society for the Promotion of Science: 17K06016

References

1. J. B. Goodenough, *Annu. Rev. Mater. Res.*, **33**, 91 (2003).
2. L. Malavasi, C. J. Fisher, and M. S. Islam, *Chem. Soc. Rev.*, **39**, 4370 (2010).
3. T. Esaka, T. Minaai, and H. Iwahara, *Denki Kagaku* (presently *Electrochemistry*), **59**, 343 (1991).
4. T. Esaka, T. Minaai, and H. Iwahara, *Solid State Ionics*, **57**, 319 (1992).
5. T. Esaka, *Solid State Ionics*, **136–137**, 1 (2000).
6. S. Takai, M. Satou, T. Yoshida, N. Chikashige, T. Kita, and T. Esaka, *Electrochemistry*, **79**, 696 (2011).
7. J. Cheng, W. Bao, C. Han, and W. Cao, *J. Power Sources*, **195**, 1849 (2010).
8. P. Jena, N. Nallamuthu, M. Venketswarulu, and N. Satyanarayana, *Ceram. Int.*, **40**, 2349 (2014).
9. R. J. Packer, E. V. Tsipis, C. N. Munnings, V. V. Kharton, S. J. Skinner, and J. R. Frade, *Solid State Ionics*, **177**, 2059 (2006).
10. C. Li, R. D. Bayliss, and S. J. Skinner, *Solid State Ionics*, **262**, 530 (2014).
11. C. Ferrara, A. Mancini, C. Ritter, L. Malavasi, and C. Tealdi, *J. Mater. Chem. A*, **3**, 22258 (2015).
12. R. Kawaguchi, R. Akizawa, Y. J. Shan, K. Tezuka, and T. Katsumata, *Solid State Ionics*, **355**, 115415 (2020).
13. S. Takai, Y. Morishita, Y. Kondo, T. Yao, T. Yabutsuka, and T. Esaka, *J. Ceram. Soc. Jpn.*, **124**, 819 (2016).
14. S. Takai, S. Shitaune, T. Sano, H. Kawaji, T. Yabutsuka, T. Esaka, and T. Yao, *Materials*, **11**, 1092 (2018).
15. F. S. Galasso, *Structure and properties of Inorganic Solids*, International Series of Monographs in Solid State Physics, Vol. 7, Pergamon, Oxford (1970).
16. X. Yang, A. J. Fernández-Carrión, J. Wang, F. Porcher, F. Fayon, M. Allix, and X. Kuang, *Nat. Commun.*, **9**, 4484 (2018).
17. S. Takai, S. Touda, K. Oikawa, K. Mori, S. Torii, T. Kamiyama, and T. Esaka, *Solid State Ionics*, **148**, 123 (2002).
18. J. Wang, L. Zhou, Y. Wang, J. Xu, X. Yang, and X. Kuang, *J. Solid State Chem.*, **268**, 16 (2018).
19. K. Toyoura, Y. Sakakibara, T. Yokoi, A. Nakamura, and K. Matsunaga, *J. Mater. Chem. A*, **6**, 12004 (2018).
20. M. Yoshimura, F. Sibieudo, A. Rouanet, and H. Foex, *Rev. Int. Hautes Temp. Refract.*, **12**, 215 (1975).